ELSEVIER

Coordination Chemistry Reviews
219–221 (2001) 937–955

COORDINATION CHEMISTRY REVIEWS

www.elsevier.com/locate/ccr

Resonance Raman spectra of d^6 metal–diimine complexes reflect changes in metal–ligand interaction and character of electronic transition

Joris van Slageren [a], Axel Klein [b], Stanislav Záliš [c], Derk J. Stufkens [a,*]

[a] *Institute of Molecular Chemistry, Universiteit van Amsterdam, Nieuwe Achtergracht 166, NL-1018 WV Amsterdam, Netherlands*
[b] *Institut für Anorganische Chemie, Universität Stuttgart, Pfaffenwaldring 55, D-70569 Stuttgart, Germany*
[c] *J. Heyrovský Institute of Physical Chemistry, Academy of Sciences of the Czech Republic, Dolejškova 3, CZ-182 23 Prague 8, Czech Republic*

Received 25 October 2000; received in revised form 4 April 2001; accepted 16 April 2001

Contents

* Corresponding author. Tel.: +31-20-525-6451; fax: +31-20-525-6456.
E-mail address: stufkens@anorg.chem.uva.nl (D.J. Stufkens).

PII: S0010-8545(01)00388-5

Abstract

This article reports the results of a comparative resonance Raman (rR) study of low-valent d^6 transition-metal α-diimine complexes. The α-diimine ligand used is *N*,*N*′-diisopropyl-1,4-diaza-1,3-butadiene (^{i}Pr-DAB) which has a relatively simple structure and hence only a few vibrations. This simplifies the assignment of the vibrational spectra of complexes of this ligand. With the help of DFT calculations of the frontier orbitals and vibrational frequencies of (model) complexes, the rR bands are assigned unambiguously. Their frequencies and intensities are discussed in terms of the electronic structures of the complexes. Comparison of the rR data demonstrates how these spectra can be used to establish changes in the metal–ligand interaction and in the character of the charge transfer transitions of these complexes.

Keywords: Diimine complexes; d^6 Transition metals; Methyl complexes; Metal–metal bonds; Resonance Raman spectra; DFT calculations

1. Introduction

Most of the early experimental data on molecular vibrations were provided by Raman spectroscopy, but this technique stagnated when commercial infrared spectrometers became available in the 1940s. The discovery of the laser as a powerful monochromatic light source and the development of sensitive detectors in the 1960s initiated the renaissance of Raman spectroscopy. In addition, contrary to the light sources used earlier, lasers and dye-lasers made the recording of so-called resonance Raman (rR) spectra viable [1–6]. Such rR spectra show enhancement of intensity of some Raman bands when the frequency of the exciting light approaches that of a strongly allowed electronic transition. If, as is usually the case, the ground state wavefunction is totally symmetric, only bands due to totally symmetric vibrations are resonantly enhanced. In addition, the Raman intensity of a vibration increases with increasing displacement along its normal coordinate of the potential energy curve of the excited state with respect to that of the ground state. In other words, the intensities are highest for those vibrations, which are most strongly coupled to that particular electronic transition. Although absorption bands of molecules contain information about all the displaced normal modes, they normally show up as an unresolved envelope in condensed media when many modes are displaced. In contrast, rR 'excitation profiles' (EP), which represent the rR intensity of a specific vibration as a function of the wavelength of excitation, provide instead information about the displacement of individual modes. EPs of many inorganic

complexes were successfully analysed by Zink et al. [6,7] in terms of excited state distortions with the time-dependent theory of Lee et al. [8–10]. Thus, rR spectra do not only provide the vibrational frequencies of a molecule in its ground state but also characterise its allowed electronic transitions by giving valuable information about the involvement of individual vibrations in these transitions.

For many years, we have applied the rR technique to assign and characterise the low-energy electronic transitions of low-valent transition metal α-diimine complexes [11–16]. The main aim of these studies was to determine the changes in structure caused by the electronic transitions and to relate these changes to the photochemical and photophysical behaviour of the complexes. However, most rR bands could only be assigned qualitatively, since a complete vibrational analysis of the complexes was too complicated at the time. Partly due to increasing computer processor speeds, quantum chemical calculations have recently improved to such an extent that they can now provide unambiguous assignments of vibrational spectra, even for complicated systems.

In view of this development and in order to obtain comparative rR data of a series of d^6 metal–α-diimine complexes differing in their ground- and/or excited-state bonding properties, we recorded the rR spectra of several of these complexes under the same conditions. All complexes under study (Fig. 1) contain the same α-diimine ligand *N*,*N*′-diisopropyl-1,4-diaza-1,3-butadiene (^{i}Pr-DAB). This ligand was chosen since it has relatively few vibrations due to its simple structure. At the same time, DFT B3LYP calculations were performed on the free ligand and several (model) complexes. It will be shown that by thorough comparison of the rR spectra of these complexes in combination with the results of the DFT calculations, most rR bands can be assigned. Furthermore, the influences of the character of the electronic transition and of the metal–ligand interaction on the rR spectra can be separated and understood.

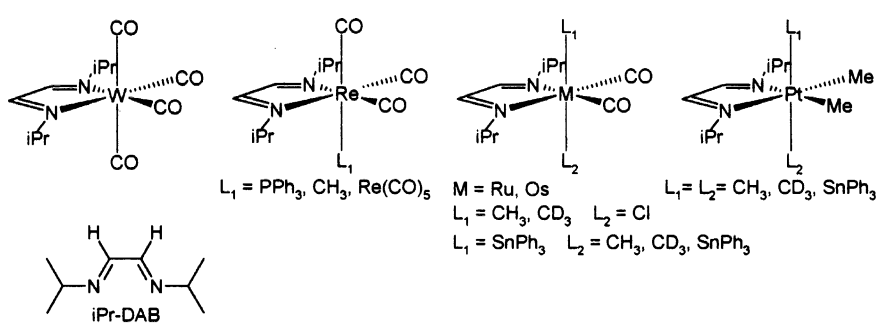

Fig. 1. Schematic structures of ligand and complexes under study.

2. Experimental

Triphenylphosphine (PPh_3, Aldrich), [$W(CO)_6$] (Strem), neutral alumina (Fluka) and $AgNO_3$ (Aldrich) were used as received. Solvents purchased from Acros (dichloromethane, pentane, tetrahydrofuran, toluene), were dried on and distilled from the appropriate drying agent under N_2, shortly before use.

All syntheses were performed under a nitrogen atmosphere using standard Schlenk techniques. ^{i}Pr-DAB [17], [$Ru(Cl)(R)(CO)_2(^i$Pr-DAB)] [13,15,18], [$Ru(SnPh_3)(R)(CO)_2(^i$Pr-DAB)] [19], [$Pt(R)_4(^i$Pr-DAB)] ($R = CH_3$, CD_3) [20,21], [$M(SnPh_3)_2(CO)_2(^i$Pr-DAB)] (M = Ru, Os) [19,22], [$Pt(SnPh_3)_2(CH_3)_2(^i$Pr-DAB)] [21], [$Ru\{RuCp(CO)_2\}_2(CO)_2(^i$Pr-DAB)] [23], were synthesised according to published procedures.

[$Re(PPh_3)(CO)_3(^i$Pr-DAB)](NO_3) was prepared by stirring [$Re(Br)(CO)_3(^i$Pr-DAB)] with one equivalent of $AgNO_3$ and an excess of PPh_3 in CH_2Cl_2. Filtration, evaporation of the solvent and washing with pentane afforded the pure product in near quantitative yield. IR (THF, cm^{-1}): 2027, 1927, 1908. ^{1}H-NMR ($CDCl_3$): δ 1.50 (d, 12H, $^3J = 6.6$ Hz, $CH(CH_3)_2$), 4.22, (septet, 12H, $^3J = 6.6$ Hz, $CH(CH_3)_2$), 7.3–7.5 (m, 15H, PPh_3), 8.61 (s, 2H, imine H) ppm.

[$W(CO)_4(^i$Pr-DAB)] was prepared by refluxing [$W(CO)_6$] and 1.1 equivalent of ^{i}Pr-DAB overnight in toluene. Flash column chromatography over neutral alumina yielded a mixture of product and starting compound, the latter of which was removed by sublimation (30 °C) in vacuo. IR (CH_2Cl_2, cm^{-1}): 2013, 1909, 1843. ^{1}H-NMR ($CDCl_3$): δ 1.56 (d, 12H, $^3J = 6.6$ Hz, $CH(CH_3)_2$), 4.29, (septet, 2H, $^3J = 6.6$, $CH(CH_3)_2$), 8.59 (s, 2H, imine H) ppm.

Resonance Raman spectra of the complexes dispersed in KNO_3 pellets were recorded on a Dilor XY spectrometer equipped with a Wright Instruments CCD detector, using a Spectra Physics 2040E Ar^+ laser in combination with Coherent CR490 and CR590 dye lasers (with Coumarin 6 and Rhodamine 6G dyes) as excitation sources under a 180° backscattering geometry. The pellet was spun in order to minimise thermal and photochemical decomposition. Data acquisition was controlled by Dilor Labspec 2.08 software. The spectra were calibrated using the Raman bands due to the symmetrical stretching and in plane bending vibrations of NO_3^- (at 1051 and 716 cm^{-1}, respectively) [24] and corrected for baseline deviations using Grams software.

In order to simplify the calculations of the ground state electronic structures of the complexes, the ^{i}Pr-DAB and $SnPh_3$ ligands were replaced by Me-DAB and SnH_3, respectively. A comparative calculation on several of the complexes showed that the replacement of ^{i}Pr-DAB by Me-DAB changes the composition of the frontier orbitals by less than 1%. The electronic structures of the model complexes [$W(CO)_4$(Me-DAB)], [$Ru(Cl)(CH_3)(CO)_2$(Me-DAB)], [$Ru(SnH_3)(CH_3)(CO)_2$(Me-DAB)], [$Pt(CH_3)_4$(Me-DAB)], [$Pt(SnH_3)_2(CH_3)_2$(Me-DAB)] and [$M(SnH_3)_2(CO)_2$(Me-DAB)] (M = Ru, Os) were calculated by density functional theory (DFT) methods using the ADF 1999 [25,26] program package and GAUSSIAN 98 [27]. Within GAUSSIAN 98, Dunning's polarised valence double ζ basis sets [28] were used for C, N, O, Cl and H atoms and the quasi-relativistic effective core

pseudopotentials and corresponding optimised set of basis functions [29] for Ru, W, Os, Pt and Sn. In these calculations, the hybrid Becke's three parameter functional with the Lee, Yang and Parr correlation functional (B3LYP) [30] were used. Within the ADF program, Slater type orbital (STO) basis sets of triple ζ quality with 3d polarisation functions for C, N and O and additional p functions for metals were employed. The inner shells were represented by a frozen core approximation, viz. 1s for C, N, O, 1s–2p for Cl, 1s–3d for Ru, 1s–4d for Os, 1s–4f for Pt and 1s–4p for Sn were kept frozen. The following density functionals were used within ADF: a local density approximation (LDA) with VWN parametrisation of electron gas data or a functional including Becke's gradient correction [31] to the local exchange expression in conjunction with Perdew's gradient correction [32] to the LDA expression (BP). The scalar relativistic (SR) zero-order regular approximation (ZORA) was used within this study.

GAUSSIAN 98 was used to calculate the vibrational frequencies of *cis*- and *trans*-^{i}Pr-DAB and [$W(CO)_4$(^{i}Pr-DAB)], and of the model complexes [$W(CO)_4$(Me-DAB)], [Ru(Cl)(R)$(CO)_2$(Me-DAB)] (R = CH_3, CD_3), [Ru(SnH_3)(CH_3)$(CO)_2$(Me-DAB)], [Pt$(R)_4$(Me-DAB)] (R = CH_3, CD_3), [Pt$(SnH_3)_2(CH_3)_2$(Me-DAB)], [Ru$(SnH_3)_2(CO)_2$(^{i}Pr-DAB)] and [M$(SnH_3)_2(CO)_2$(Me-DAB)] (M = Ru, Os). Frequency calculations were done at G98/B3LYP optimised geometries. Energy minima were characterised either by a nonexistence of imaginary frequencies or very low imaginary frequencies corresponding to the methyl/SnH_3 rotational motion only. Problematic cases were solved by using the ultra fine grid in the DFT procedure.

All calculations, except for [Ru(Cl)(CH_3)$(CO)_2$(Me-DAB)] and [Ru(SnH_3)-(CH_3)$(CO)_2$(Me-DAB)], were performed on the complexes in constrained C_{2v} symmetry, with the z-axis coincident with the C_2 symmetry axis. The R-DAB ligand and the C atoms of the equatorial CO/CH_3/CD_3 groups are located in the yz-plane, and the SnH_3/CH_3/CD_3 axial ligands lie on the x-axis. Calculations on [Ru(Cl)(CH_3)$(CO)_2$(Me-DAB)] and [Ru(SnH_3)(CH_3)$(CO)_2$(Me-DAB)] were performed in constrained C_s symmetry, with the z-axis bisecting the DAB ligand as above. The calculated vibrational frequencies are collected in Table 1, the calculated one-electron energies of the MOs and their compositions are presented in Table 2.

3. Influence of metal–diimine π-backbonding

3.1. The ^{i}Pr-DAB ligand

The Raman spectrum of ^{i}Pr-DAB was obtained by excitation at 514.5 nm of a CH_2Cl_2 solution of the freshly sublimed free ligand, rather than dispersed in a KNO_3 pellet, in order to prevent sublimation by the laser beam. To assist in the assignment, the vibrations of this ligand were calculated, both in its *cis*- and *trans*-geometry. The main band is observed at 1636 cm^{-1} (Table 1) and attributed to the symmetrical stretching vibration of the CN bonds, ν_s(CN). It is calculated

Table 1
Main rR bands of the ^{i}Pr-DAB complexes under study.

Compound	ν_s(CO)	ν_s(CN)	δ_s(CH)	δ_s(Me)	δ_s(DAB)		δ_s(MCO)	ν_s(MC)	ν_s(MN)
^{i}Pr-DAB		1636							
		(1693)							
[Re(PPh$_3$)(CO)$_3$(^{i}Pr-DAB)]$^+$	2025	1557							
[W(CO)$_4$(^{i}Pr-DAB)]	2017	1499	1147		931	847	623	432	222
	(2089)	(1545)	(1133)				(610)	(431)	(216)
	(2084) [a]	(1531)	(1176)		(960)	(830)	(616)	(427)	(227)
[Re(CH$_3$)(CO)$_3$(^{i}Pr-DAB)]	1988	1511	1359	1156				451	
[Ru(Cl)(CH$_3$)(CO)$_2$(^{i}Pr-DAB)]	2017	1573		1209				492	
	(2110)	(1626)		(1269)				(500)	
[Ru(Cl)(CD$_3$)(CO)$_2$(^{i}Pr-DAB)]	2016	1573		924				490	
	(2109)	(1626)		(962)				(496)	
[Ru(SnPh$_3$)(CH$_3$)(CO)$_2$(^{i}Pr-DAB)]		1492	1296	1156	950	836	610		241
		(1551)	(1413)	(1220)			(696)		(235)
[Ru(SnPh$_3$)(CD$_3$)(CO)$_2$(^{i}Pr-DAB)]		1490	1296	884	948	835	604		
[Pt(CH$_3$)$_4$(^{i}Pr-DAB)]		1564		1175					
		(1602)		(1213)					
[Pt(CD$_3$)$_4$(^{i}Pr-DAB)]		1567		894					
		(1590)		(923)					
[Ru(Cl)(SnPh$_3$)(CO)$_2$(^{i}Pr-DAB)]		1543					605	478	
[Re{Re(CO)$_5$}(CO)$_3$(^{i}Pr-DAB)]		1467	1289		957	838			
[Pt(SnPh$_3$)$_2$(CH$_3$)$_2$(^{i}Pr-DAB)]		1474	1292		949	834			
		(1552)	(1410)						
[Ru(SnPh$_3$)$_2$(CO)$_2$(^{i}Pr-DAB)]		1473	1283		953	836	610	419	250
		(1541)	(1405)				(601)	(478)	(238)
		(1528) [b]	(1327)		(971)	(836)	(650)	(490)	
[Os(SnPh$_3$)$_2$(CO)$_2$(^{i}Pr-DAB)]		1472	1278		959	842	610	418	
		(1540)	(1393)				(641)	(480)	
[Ru{RuCp(CO)$_2$}$_2$(CO)$_2$(^{i}Pr-DAB)]		1473	1280		958	832	606	405	

Assignments include major contributions only, for details see text. The calculated values between brackets are for model complexes in which the ^{i}Pr-DAB and SnPh$_3$ ligands were replaced by Me-DAB and SnH$_3$, respectively, unless indicated otherwise.

[a] [W(CO)$_4$(^{i}Pr-DAB)].

[b] [Ru(SnH$_3$)$_2$(CO)$_2$(^{i}Pr-DAB)].

Table 2
ADF calculated one-electron energies and percentage composition of the frontier molecular orbitals (expressed in terms of composing fragments) mainly involved in the lowest-energy allowed CT transitions of the model complexes $[M(L_{ax1})(L_{ax2})(L_{eq})_2(R\text{-}DAB)]$.

	MO (symmetry)	E (eV)	M	L_{ax1}	L_{ax2}	L_{eq} (total)	DAB (π*)
$[W(CO)_4(Me\text{-}DAB)]$	LUMO (b_1)	−3.73	9(d_{xz})	7	7	8	68
	HOMO (b_1)	−5.52	42 (d_{xz})	11	11	5	31
$[Ru(Cl)(CH_3)(CO)_2(Me\text{-}DAB)]$	LUMO (a′)	−3.92	7(d_{xz}); 1 (p_z)	6	3	4	79
	HOMO (a′)	−5.23	20 (d_{xz})	71	1	2	5
$[Ru(SnH_3)(CH_3)(CO)_2(Me\text{-}DAB)]$ [a]	LUMO (a′)	−3.44	10 (d_{xz}); 1 (p_x)	14	7	1	67
	HOMO (a′)	−5.30	12 (p_x); 1(d_{xz})	33	22	6	26
$[Pt(CH_3)_4(Me\text{-}DAB)]$	LUMO (b_1)	−3.40	8(d_{xz}); 1 (p_x)	7	7	–	77
	HOMO (b_1)	−4.83	9 (p_x); 1(d_{xz})	37	37	3	13
$[Pt(SnH_3)_2(CH_3)_2(Me\text{-}DAB)]$	LUMO (b_1)	−3.57	5(d_{xz}); 1 (p_x)	12	12	–	71
	HOMO (b_1)	−4.92	10 (p_x); 1(d_{xz})	30	30	6	18
$[Ru(SnH_3)_2(CO)_2(Me\text{-}DAB)]$ [b]	LUMO (b_1)	−3.61	9 (d_{xz}); 1 (p_x)	12	12	–	66
	HOMO (b_1)	−5.57	13 (p_x); 1(d_{xz})	26	26	8	27
$[Os(SnH_3)_2(CO)_2(Me\text{-}DAB)]$	LUMO (b_1)	−3.50	9 (d_{xz}); 1 (p_x)	12	12	–	66
	HOMO (b_1)	−5.63	16 (p_x); 2(d_{xz})	25	25	5	27

The axial ligands are on the x-axis of the complex.

[a] For calculations on the respective H-DAB model complexes see Ref. [14].

[b] For calculations on the respective H-DAB model complexes see Ref. [47].

about 3% too high (at 1693 cm^{-1} for both isomeric structures of ^{i}Pr-DAB), but such a difference between calculated and observed frequencies is quite normal for DFT calculations with B3LYP functionals and double ζ basis sets [33]. In addition, a number of weaker bands are found.

The ^{i}Pr-DAB ligand has a low-lying π^* orbital, while low-valent transition metal atoms have high-lying filled metal-d orbitals. Because of this, the complexes formed between such a metal and a chelating ^{i}Pr-DAB ligand normally possess low-energy metal-to-ligand charge transfer (MLCT) transitions. Such an MLCT transition first of all affects the bonds and vibrations of ^{i}Pr-DAB and to a lesser extent those of the co-ligands. The strength of the metal–ligand interaction determines which vibrations are influenced by an MLCT transition as will be shown by the rR spectra of two representative complexes.

3.2. *[Re(PPh$_3$)(CO)$_3$(^{i}Pr-DAB)]$^{+}$*

As the first example of a complex with a lowest MLCT transition [Re(PPh$_3$)(CO)$_3$(^{i}Pr-DAB)](NO$_3$) was selected rather than the well known complex [Re(Cl)(CO)$_3$(^{i}Pr-DAB)]. In the latter complex the chloride ligand orbitals participate in the highest filled orbitals, and because of this the lowest-energy electronic transition does not have purely MLCT character. This is evidenced by the observation of ν(Re–Cl) in the rR spectrum of this complex [12,34]. The rR spectrum of [Re(PPh$_3$)(CO)$_3$(^{i}Pr-DAB)]$^{+}$ in [Re(PPh$_3$)(CO)$_3$(^{i}Pr-DAB)](NO$_3$), obtained by excitation into its lowest-energy absorption band, only shows two resonantly enhanced Raman bands (Fig. 2). The more intense band found at 1557 cm^{-1} is attributed to ν_s(CN). It is ca. 80 cm^{-1} lower in frequency than observed for the free ligand, due

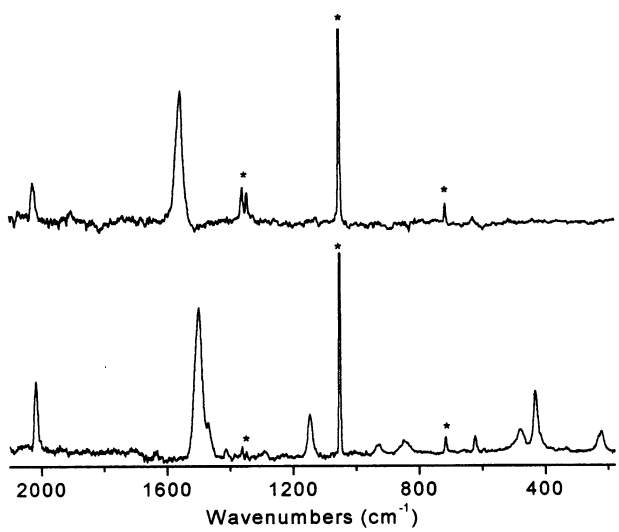

Fig. 2. RR spectra of [Re(PPh$_3$)(CO)$_3$(^{i}Pr-DAB)]$^{+}$ (top, $\lambda_{exc} = 457.9$ nm) and [W(CO)$_4$(^{i}Pr-DAB)] (bottom, $\lambda_{exc} = 514.5$) in KNO$_3$. Asterisks denote NO_3^- bands.

to dπ(Re)–π*(^{i}Pr-DAB) π-backbonding. Since the π* orbital is antibonding with respect to the CN bonds, the frequency of ν_s(CN) is lower for the complex than for the free ligand. The MLCT transition increases the electron density in the π*(^{i}Pr-DAB) orbital even more. Hence, this transition affects the CN stretching mode and causes a resonance enhancement of Raman intensity for this vibration. The other resonantly enhanced band at 2025 cm^{-1} belongs to the in-phase symmetric vibration ν_s(CO) of the three carbonyls [35]. Its rR effect is caused by the oxidation of the metal and concomitant decrease of metal–CO π-backbonding during the electronic transition.

3.3. [W(CO)$_4$(^{i}Pr-DAB)]

Going from Re(I) to W(0) the metal d-orbital energy is raised, causing an increase of the metal-to-^{i}Pr-DAB π-backbonding. In the rR spectrum this is manifested by a lowering of the ν_s(CN) frequency from 1557 to 1499 cm^{-1} (Fig. 2). The calculated frequency for this vibration is 1531 cm^{-1}. Since the metal atom is oxidised during the electronic transition, the in-phase symmetric mode of the carbonyls [36], ν_s(CO), is again resonantly enhanced and observed at 2017 cm^{-1} (calculated at 2089 cm^{-1}). However, a number of extra bands are observed (at 1147, 931, 847, 624, 480, 432 and 222 cm^{-1}), which are not present in the spectrum of the Re complex. These bands can be assigned with the aid of the DFT vibrational calculations (Table 1). The band at 1147 cm^{-1} was observed at 1150 cm^{-1} for [Mo(CO)$_4$(^{i}Pr-DAB)] [37,38]. Based on the DFT calculations of [W(CO)$_4$(R-DAB)] (R = Me, ^{i}Pr) it is assigned to a combined ν(CC)/δ_s(CH) vibration, where δ_s(CH) is an in-plane symmetric movement of the two imine hydrogen atoms. For R = Me, ν(CC)/δ_s(CH) is calculated at 1133 cm^{-1}, for R = ^{i}Pr at 1176 cm^{-1}. Note that the frequency of this vibration strongly depends on R, an effect that has been found for all complexes under study (vide infra). The latter value is again somewhat higher than the frequency of the band observed in the rR spectrum of [W(CO)$_4$(^{i}Pr-DAB)] (1147 cm^{-1}). The observation of this rR band in the spectrum of the W complex and its absence in the spectrum of the corresponding Re compound indicate that the central CC bond is only affected by the MLCT transition if there is a strong dπ–π* interaction in the ground state. The bands found at 931 and 847 cm^{-1} (calculated at 960 and 830 cm^{-1}, respectively, for [W(CO)$_4$(^{i}Pr-DAB)]) are assigned to in-plane deformation modes of the ligand. These two deformation modes are not correctly calculated if the ^{i}Pr-DAB ligand is simplified to Me-DAB in this and the other complexes under study. The band found at 623 cm^{-1} and calculated at 616 cm^{-1} is due to a δ_s(WCO) mode, while the ones observed at 480 and 431 cm^{-1} (calculated at 449 and 427 cm^{-1}, respectively) belong to combined ν_s(W–C) and ν_s(W–N) stretching modes. Additionally, the band at 222 cm^{-1} has been attributed to ν_s(W–N) on the basis of isotope labelling studies [38], and is calculated at 227 cm^{-1}. The appearance of these extra rR bands on going from the Re to the W complex is caused by the increase of interaction between the dπ(M) and π*(^{i}Pr-DAB) orbitals involved in the main MLCT transition. The strong interaction in the case of [W(CO)$_4$(^{i}Pr-DAB)]

agrees with the large calculated contribution of the π*(^{i}Pr-DAB) orbital to its HOMO (Table 2). As a result the transition has less charge transfer character and obtains partial metal–ligand bonding-to-antibonding character. Such a transition causes a weakening of the metal–nitrogen bonds and invokes rR effects for ν_s(W–N) [37,39] and for deformation modes of the W-DAB metallacycle (see also the spectra presented in Fig. 5 and discussed in Section 5.3 and Section 5.4). The metal–nitrogen bonds are normally much less affected when the transition has more charge transfer character, since the decrease of covalent metal–nitrogen interaction is then compensated by an increase of electrostatic interaction. The dπ–π* interaction can further be enhanced by increasing the metal d-orbital energy (e.g. in [Ni(CO)$_2$(^{t}Bu-DAB)]) [40], or by decreasing the π*(α-diimine) orbital energy [e.g. in W(CO)$_4$(R-DAB) (R = pTol, Mes)] [37]. The rR spectra of these complexes show much higher intensities for the metal–ligand stretching and ligand deformation modes below 1000 cm^{-1} while at the same time both ν_s(CO) and ν_s(CN) are much weaker than in the case of the Re(I) and W(0) complexes under study. In Section 5.4, we report on a complex for which ν_s(CO) and ν_s(CN) have disappeared from the rR spectrum due to a complete delocalisation of the orbitals involved in the electronic transition over the metallacycle.

So far, the co-ligands were not directly involved in the HOMO → LUMO transition. However, the situation changes when a co-ligand is introduced with high-lying filled orbitals, which contribute to the HOMO. For instance, in the case of the halide (X) complexes [Re(X)(CO)$_3$(α-diimine)] the pπ(X) orbitals contribute to the highest-filled orbitals, causing a change of character of the low-energy transitions from metal-to-ligand charge transfer to halide-to-ligand charge transfer when Cl$^-$ is replaced by I$^-$ [12]. Another ligand with a high-lying orbital is the methyl ligand. The influence of the introduction of this ligand in d^6 metal–diimine complexes on the rR spectra is discussed in Section 4.

4. Influence of methyl ligands

4.1. [Re(CH$_3$)(CO)$_3$(^{i}Pr-DAB)]

Due to the electron donating character of the methyl ligand, the lowest-energy MLCT transition of this complex is shifted to longer wavelength with respect to that of [Re(PPh$_3$)(CO)$_3$(^{i}Pr-DAB)]$^+$. Although the UV-photoelectron spectroscopic studies showed that the energy of the σ(Re–CH$_3$) orbital is only slightly lower than that of the metal-d orbitals, the rR spectra show only a small influence of the CH$_3$ group [41]. Thus, similarly to [Re(PPh$_3$)(CO)$_3$(^{i}Pr-DAB)]$^+$, both ν_s(CO) (at 1988 cm^{-1}) and ν_s(CN) (at 1511 cm^{-1}) are again observed. The shifts of these vibrations to lower frequencies compared to those of the PPh$_3$ complex, are again in correspondence with the higher electron density on the metal, leading to an increase of both the metal–CO and metal–DAB π-backbonding. A weak band at 1156 cm^{-1} is the first evidence that the CH$_3$ ligand participates in the electronic transition. In the case of [Re(R)(CO)$_3$(dmb)] (R = CH$_3$, CD$_3$; dmb = 4,4′-dimethyl-

2,2′-bipyridine) this band was found to shift from 1166 to 898 cm^{-1} going from the CH_3 to the CD_3 complex [16], and accordingly assigned to the symmetrical CH_3 deformation mode, $\delta_s(CH_3)$. A similar vibration was found for $[Re(CH_3)(CO)_5]$ [42]. The weak band at 732 cm^{-1} is assigned to the corresponding rocking mode of the CH_3 group, $\rho(CH_3)$. Further bands are observed at 503, 488 and 451 cm^{-1}, all of which are very weak and belong to metal–ligand stretching and deformation modes, probably similar to the ones found for $[W(CO)_4(^i$Pr-DAB)]. In conclusion, the rR spectrum of $[Re(CH_3)(CO)_3(^i$Pr-DAB)] is very similar to that of $[Re(PPh_3)(CO)_3(^i$Pr-DAB)]$^+$, and the methyl ligand of the former complex is only weakly involved in the charge transfer transition.

4.2. *[Ru(Cl)(R)(CO)$_2$(^{i}Pr-DAB)] (R = CH$_3$, CD$_3$)*

RR spectra were recorded for the complexes $[Ru(Cl)(R)(CO)_2(^i$Pr-DAB)] (R = CH_3, CD_3) [13,15] (Fig. 3) and DFT vibrational calculations were performed on the model complexes $[Ru(Cl)(R)(CO)_2$(Me-DAB)] (R = CH_3, CD_3). The rR spectra (Fig. 3) are very similar to those of the Re–methyl complex discussed above. Thus, ν_s(CO) is observed at 2016 cm^{-1} (calculated at 2110 cm^{-1} for the model complex) and ν_s(CN) at 1573 cm^{-1} (calculated at 1626 cm^{-1}). The high frequency of ν_s(CN) points to a weak metal–ligand π-interaction which is also evident from the small calculated contribution of π*(R-DAB) to the HOMO (Table 2). Note the very large calculated contribution of the chloride to this orbital. Similar values were found with the DFT method for other metal–halide complexes and are most likely too

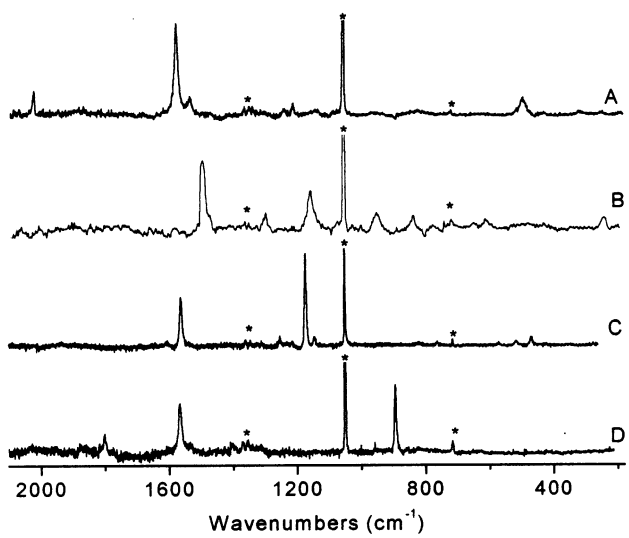

Fig. 3. RR spectra of: (A) $[Ru(Cl)(CH_3)(CO)_2(^i$Pr-DAB)] (λ_{exc} = 457.9 nm); (B) $[Ru(CH_3)(SnPh_3)$-$(CO)_2(^i$Pr-DAB) (λ_{exc} = 488.0 nm); (C) $[Pt(CH_3)_4(^i$Pr-DAB)] (λ_{exc} = 591.0 nm); and (D) $[Pt(CD_3)_4(^i$Pr-DAB)] (λ_{exc} = 545.0 nm) in KNO_3. Asterisks denote NO_3^- bands.

high [14,43,44]. Due to the small metal–ligand π-interaction the HOMO → LUMO transition has much charge transfer character, which agrees with the large solvatochromic shift ($\Delta = \nu(\text{MeCN}) - \nu(\text{toluene}) = 1870\ \text{cm}^{-1}$) of the absorption band [13].

In addition, a weak Raman band is observed at 1209 cm^{-1} (calculated at 1269 cm^{-1}) which shifts to 924 cm^{-1} (calculated at 962 cm^{-1}) on deuteration of the methyl group. Again, this band is attributed to $\delta_s(CH_3/CD_3)$. A strongly enhanced band is observed at ca. 490 cm^{-1} for both the CH_3 and CD_3 complex. For the [Ru(I)(R)$(CO)_2$(^{i}Pr-DAB)] complexes, this band was assigned to ν_s(Ru–CO) and not to ν(Ru–CH_3), as its frequency did not shift on deuteration of the methyl group [15]. The present calculations show that this normal mode (calculated at 500 cm^{-1}, observed at 492 cm^{-1}) has ν_s(Ru–N) and ν_s(Ru–CO) character with a ν(Ru–CH_3) contribution for the CH_3 complex. According to the calculations, ν(Ru–CD_3) does not contribute to this normal mode in the CD_3 complex, which is calculated at 496 cm^{-1} and observed at 490 cm^{-1}.

4.3. [Ru($SnPh_3$)(R)$(CO)_2$(^{i}Pr-DAB)] (R = CH_3, CD_3)

Replacement of Cl^- by an $SnPh_3$ ligand drastically changes the electronic structure of these complexes. The methyl and $SnPh_3$ ligands are in axial position and according to the calculations on the model complex [Ru(SnH_3)(CH_3)$(CO)_2$(Me-DAB)] the HOMO has a σ(Sn–Ru–C) character and consists of the antisymmetric combination of the sp^3 orbitals of the axial ligands, of p(Ru) and π*(Me-DAB) (Table 2). The main difference with the preceding complexes is that instead of dπ(Ru), σ(Sn–Ru–C) is responsible for the π-interaction with ^{i}Pr-DAB and that the electronic transition has σ(Sn–Ru–C) → π*(^{i}Pr-DAB) or sigma-bond-to-ligand charge transfer (SBLCT) instead of dπ(Ru) → π*(^{i}Pr-DAB) (MLCT) character. The σ–π* interaction is rather strong and lowers the frequency of ν_s(CN) to 1492 cm^{-1}. The electronic transition mainly involves transfer of negative charge from the axial ligands without an appreciable effect on the charge density at the central metal atom and the carbonyl ligands. This agrees with the absence of a ν_s(CO) band in the rR spectra.

As shown hereinafter, the rR spectra of these and other methyl complexes with a lowest SBLCT state are different from those discussed before. For the assignment of the rR bands of this complex (Fig. 3, Table 1), the DFT calculated vibrations of the model complex [Ru(SnH_3)(CH_3)$(CO)_2$(Me-DAB)] were used. The deformation mode of the CH_3 ligand, $\delta_s(CH_3)$, is found at 1156 cm^{-1} (calculated 1209 cm^{-1}) and it shifts to 884 cm^{-1} on deuteration. The strong rR effect of this vibration is due to the fact that the SBLCT transition lowers the electron density in the σ(Sn–Ru–C) orbital, causing a change of the methyl bonds and angles and accordingly a rR effect for $\delta_s(CH_3)$. In the case of [Ru(Cl)(CH_3)$(CO)_2$(^{i}Pr-DAB)] the rR effect of $\delta_s(CH_3)$ is weaker, since the methyl ligand of this complex has only a minor contribution to the HOMO and to the lowest MLCT transition. The low frequency of ν_s(CN) (observed at 1491 cm^{-1} and calculated at 1563 cm^{-1}) and the appearance of δ_s(DAB) deformation vibrations at 950 and 836 cm^{-1} point again to a strong π-backbonding, just as in the case of [W$(CO)_4$(^{i}Pr-DAB)] (vide supra).

In addition, however, a new (weak) band shows up at 1296 cm^{-1}. According to the calculations, it mainly consists of a symmetric in-plane movement of the imine hydrogen atoms, coupled to the symmetric CN-stretching vibration. Fig. 4 shows a pictorial representation of this vibration, which will be denoted as δ_s(CH). Just as in the case of ν(CC)/δ(CH) of the complexes [$W(CO)_4$(R-DAB)] (vide supra), the large difference between the frequency of δ_s(CH) observed for the real complex [$Ru(SnPh_3)(CH_3)(CO)_2$(^{i}Pr-DAB)] (1296 cm^{-1}) and the frequency calculated for the model complex [$Ru(SnH_3)(CH_3)(CO)_2$(Me-DAB)] (1413 cm^{-1}) is caused by the sensitivity of this frequency to the substituents R of the R-DAB ligand. Further bands are observed at 610 and 241 cm^{-1} (calculated at 618 and 239 cm^{-1}), which, according to the calculations, belong to δ_s(RuCO) and ν_s(Ru–N).

4.4. [$Pt(R)_4$(^{i}Pr-DAB)] (R = CH_3, CD_3)

The two axial methyl groups of this complex contribute to two σ(C–Pt–C) orbitals. One of these is the HOMO which consists of the antisymmetric combination of the axial methyl sp^3 orbitals, of π*(^{i}Pr-DAB), and a minor contribution from a p(Pt) orbital (Table 2) [20,21,45]. The rR spectra, obtained by excitation into the SBLCT transition of [$Pt(R)_4$(^{i}Pr-DAB)] (R = CH_3, CD_3) (Fig. 3) are interpreted with the help of DFT calculations on the [$Pt(R)_4$(Me-DAB)] (R = CH_3, CD_3) model complexes [21].

Two major bands are found in the rR spectra. First of all, ν_s(CN) is observed at ca. 1565 cm^{-1} (calc. at ca. 1595 cm^{-1}) for both the CH_3 and CD_3 complexes (Table 1). However, the most intense rR band is found at 1175 cm^{-1} for the CH_3 complex and at 894 cm^{-1} for the CD_3 complex. This band is again assigned to the symmetrical deformation of the methyl groups, $\delta_s(CH_3/CD_3)$, on the basis of the shift on deuteration. Moreover, the calculated frequencies (1213 and 923 cm^{-1}, respectively) for this vibration in the CH_3 and CD_3 model complexes, agree with the observed values (1175 and 894 cm^{-1}). The rR intensity of $\delta_s(CH_3/CD_3)$ is much higher for these complexes than for [$Re(CH_3)(CO)_3$(^{i}Pr-DAB)] and [$Ru(Cl)(R)(CO)_2$(^{i}Pr-DAB)] (R = CH_3, CD_3). This agrees with the results from DFT calculations that in [$Pt(CH_3)_4$(Me-DAB)] the σ(CH_3) orbitals are the main contributors to the HOMO from which the SBLCT transition originates (Table 2) [21]. For [$Pt(CH_3)_4$(^{i}Pr-DAB)], $\nu_s(Pt–C)_{eq}$ and $\nu_s(Pt–C)_{ax}$ are found as very weak

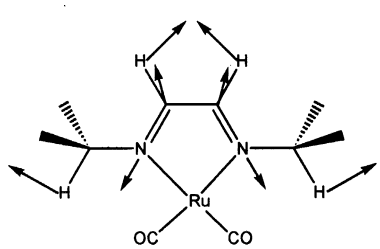

Fig. 4. Pictorial representation of the δ_s(CH) vibration.

bands at 517 and 469 cm^{-1}, respectively. Although in particular the latter vibration is expected to be vibronically coupled to the SBLCT transition, the absence of a strong rR effect for this vibration is not in line with these expectations.

5. Influence of metal–metal bonds

5.1. [Ru(Cl)($SnPh_3$)$(CO)_2$(^{i}Pr-DAB)]

Just as the methyl ligand, a metal fragment bonded to the central metal atom can affect the rR spectra in various ways, depending on the involvement of the metal–metal bonding orbital in the electronic transition in which the excitation takes place. If in the complex [Ru(Cl)(Me)$(CO)_2$(^{i}Pr-DAB)] the methyl ligand is replaced by $SnPh_3$, the rR spectrum of the resulting complex [Ru(Cl)($SnPh_3$)-$(CO)_2$(^{i}Pr-DAB)] is even simpler than that of [Ru(Cl)(Me)$(CO)_2$(^{i}Pr-DAB)], since only the Raman band belonging to ν_s(CN) is observed as a strong band. It has shifted from 1576 to 1543 cm^{-1}, pointing to an increase of π-backbonding when the methyl ligand is replaced by the $SnPh_3$ group [14,19]. The rR band belonging to ν_s(CO) has disappeared. This could imply a loss of charge transfer character, but the relatively high frequency of ν_s(CN) (1543 cm^{-1}) points to a weak metal–DAB π-backbonding. This will give rise to the transfer of an appreciable amount of charge during this transition. Hence, the disappearance of ν_s(CO) is probably due to the fact that the transition has partial XLCT (X = Cl) character [14]. In addition, very weak bands are observed at 605, 478 and 244 cm^{-1}, which belong to δ_s(RuCO), ν_s(Ru–C) and ν_s(Ru–N) respectively, in accordance with the assignment of bands at similar frequencies for e.g. [W$(CO)_4$(^{i}Pr-DAB)] (vide supra).

5.2. [Re{Re$(CO)_5$}$(CO)_3$(^{i}Pr-DAB)]

The influence of replacing a methyl group by a metal fragment is much larger when the methyl ligand in [Re$(CH_3)(CO)_3$(^{i}Pr-DAB)] is substituted by a Re$(CO)_5$ fragment. The HOMO of [Re{Re$(CO)_5$}$(CO)_3$(^{i}Pr-DAB)] was shown to be the σ(Re–Re) orbital [46], but the lowest-energy allowed transition has dπ(Re)→ π*(^{i}Pr-DAB) (MLCT) character [11]. Again, the absence of any ν(CO) band in the rR spectrum, shows the lack of charge transfer character of this transition. This points to large contributions of the dπ(Re) and π*(^{i}Pr-DAB) orbitals to the HOMO and LUMO leading to delocalisation of charge within the Re-DAB metallacycle. This delocalisation is so pronounced that ν_s(CN) (observed at 1467 cm^{-1}) has become weak. In fact the strongest bands in the rR spectrum are now the δ_s(DAB) bands at 957 and 838 cm^{-1}. The band observed at 1289 cm^{-1} is attributed to the same δ_s(CH) vibration that was observed for [Ru($SnPh_3$)(R)$(CO)_2$(^{i}Pr-DAB)] (R = CH_3, CD_3) (vide supra).

The last part of this section is devoted to trinuclear complexes. In these complexes the axial metal fragments participate in the HOMO and in the lowest-en-

ergy transition, which therefore has SBLCT character, just as in the case of $[Pt(CH_3)_4(^iPr\text{-}DAB)]$ (vide supra).

5.3. $[Pt(SnPh_3)_2(CH_3)_2(^iPr\text{-}DAB)]$ and $[M(SnPh_3)_2(CO)_2(^iPr\text{-}DAB)]$ (M = Ru, Os)

The lowest-energy electronic transition of these complexes has SBLCT character [14,21,47] just as in the case of the complexes $[Ru(SnPh_3)(CH_3)(CO)_2(^iPr\text{-}DAB)]$ and $[Pt(CH_3)_4(^iPr\text{-}DAB)]$ discussed in the previous sections. Interestingly, the frequencies of the rR bands do not shift much going from the Pt to the Ru and Os complex (Table 1), which agrees with the results from the DFT calculations on the HOMO of these complexes (Table 2) that the $SnPh_3$ ligands contribute much more to the π-bonding interaction with the ^{i}Pr-DAB ligand than the central metal atom.

For all the three complexes ν_s(CN) has a constant frequency of 1472–1474 cm^{-1}, while that of δ_s(CH) varies between 1278 and 1292 cm^{-1}. A comparison of the frequency of the latter vibration (1283 cm^{-1}) for $[Ru(SnPh_3)_2(CO)_2(^iPr\text{-}DAB)]$ [22] with those calculated for the model complexes $[Ru(SnH_3)_2(CO)_2(R\text{-}DAB)]$ (1405 cm^{-1} for R = Me and 1327 cm^{-1} for R = ^{i}Pr) shows again that the calculated frequency of δ_s(CH) is very sensitive to R. A much weaker band belonging to δ_s(CH) is also present in the rR spectrum of $[Ru(SnPh_3)(CH_3)(CO)_2(^iPr\text{-}DAB)]$ [14] (vide supra) and this difference in rR intensity can be explained as follows.

Going from $[Ru(SnPh_3)(CH_3)(CO)_2(^iPr\text{-}DAB)]$ to $[Pt(SnPh_3)_2(CH_3)_2(^iPr\text{-}DAB)]$ the frequency of ν_s(CN) decreases from 1492 to 1474 cm^{-1}, which points to an increase of π-backbonding i.e. of the interaction between the σ orbital and π*(^{i}Pr-DAB) [14,21]. This increase is not obvious from the calculated compositions of the HOMOs of the model complexes. However, such discrepancies between real and model complexes are not unexpected. As a result of its frequency decrease, ν_s(CN) couples to δ_s(CH), giving rise to resonance enhancement of the latter vibration at ca. 1292 cm^{-1} in the Pt complex. This increase of resonance enhancement for δ_s(CH) appears rather sudden, since the vibration is weak for $[Ru(SnPh_3)(CH_3)(CO)_2(^iPr\text{-}DAB)]$ (ν_s(CN) = 1492 cm^{-1}), but rather intense for $[Pt(SnPh_3)_2(CH_3)_2(^iPr\text{-}DAB)]$ (ν_s(CN) = 1474 cm^{-1}). Going from $[Pt(SnPh_3)_2(CH_3)_2(^iPr\text{-}DAB)]$ to $[Ru(SnPh_3)_2(CO)_2(^iPr\text{-}DAB)]$ the frequency of ν_s(CN) hardly changes, and one is tempted to conclude that the π-backbonding has not further increased. However, the SBLCT transition of $[Ru(SnPh_3)_2(CO)_2(^iPr\text{-}DAB)]$ is less solvatochromic ($\Delta = \nu$(MeCN) − ν(toluene) = 570 cm^{-1}) [22] than that of $[Pt(SnPh_3)_2(CH_3)_2(^iPr\text{-}DAB)]$ (Δ = 900 cm^{-1}) [21], which points to a decrease of charge transfer character and, accordingly, to an increase of π-backbonding i.e. of the interaction between the σ(Sn–M–Sn) and π*(^{i}Pr-DAB) orbitals involved in the SBLCT transition. However, this increase of π-backbonding does not influence the frequency of ν_s(CN) anymore but increases its coupling to δ_s(CH) as can be seen from the intensity increase and frequency lowering of the latter vibration on going from $[Pt(SnPh_3)_2(CH_3)_2(^iPr\text{-}DAB)]$ to $[Ru(SnPh_3)_2(CO)_2(^iPr\text{-}DAB)]$ (Fig. 5).

The increase of σ(Sn–M–Sn)–π*(^{i}Pr-DAB) interaction on going from $[Pt(SnPh_3)_2(CH_3)_2(^iPr\text{-}DAB)]$ to $[Ru(SnPh_3)_2(CO)_2(^iPr\text{-}DAB)]$ is also reflected in an

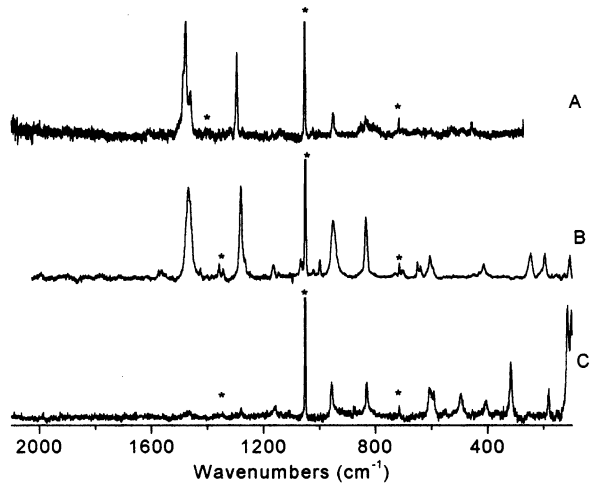

Fig. 5. RR spectra of: (A) $[Pt(SnPh_3)_2(CH_3)_2(^iPr\text{-}DAB)]$ ($\lambda_{exc} = 595.6$ nm, recorded at 90 K); (B) $[Ru(SnPh_3)_2(CO)_2(^iPr\text{-}DAB)]$ ($\lambda_{exc} = 457.9$ nm); and (C) $[Ru\{RuCp(CO)_2\}_2(CO)_2(^iPr\text{-}DAB)]$ ($\lambda_{exc} = 590.0$ nm) in KNO_3. Asterisks denote NO_3^- bands.

intensity increase of the rR bands below 1000 cm^{-1}. Although the intensities of these bands are still lower than those of the high-frequency modes, the distortion along their normal coordinates is still significant in view of their low frequencies [6,48]. These low-frequency modes are normally observed when there is a strong interaction between the metal and ligand orbitals involved in the electronic transition [37–40]. This transition then obtains less charge transfer and more metal–ligand bonding-to-antibonding character. It is reflected in a decrease of solvatochromism of the absorption band and in the observation of strong rR effects for the metal–ligand stretching modes between 200 and 600 cm^{-1}. At the same time two Raman bands between 800 and 1000 cm^{-1} increase in intensity, which, according to the calculations, belong to in-plane deformation modes of the ^{i}Pr-DAB ligand. Such a deformation of the metal–^{i}Pr-DAB metallacycle occurs when the metal–nitrogen bonds are weakened on excitation. This is the case when the transition is metal–ligand bonding-to-antibonding, but is not observed when the transition has much charge transfer character. In the latter case the decrease of covalent metal–nitrogen interaction is normally compensated by an increase of electrostatic interaction [39]. A similar effect has already been discussed for the complexes $[Re(PPh_3)(CO)_3(^iPr\text{-}DAB)]^+$ and $[W(CO)_4(^iPr\text{-}DAB)]$ (vide supra, Fig. 2). Going from the Re to the W complex the interaction between the $d\pi$(M) and $\pi^*(^iPr\text{-}DAB)$ orbitals increases, an effect which is similar to the increase of mixing between the σ(Sn–M–Sn) and $\pi^*(^iPr\text{-}DAB)$ orbitals going from $[Pt(SnPh_3)_2(CH_3)_2(^iPr\text{-}DAB)]$ to $[Ru(SnPh_3)_2(CO)_2(^iPr\text{-}DAB)]$.

5.4. [Ru{RuCp(CO)$_2$}$_2$(CO)$_2$(^{i}Pr-DAB)]

The first absorption band of this complex does not show any solvatochromism [23], which implies that the orbitals involved in the SBLCT transition are completely delocalised over the Ru–Ru–Ru moiety and the ^{i}Pr-DAB ligand. Just as in the case of [Re{Re(CO)$_5$}(CO)$_3$(^{i}Pr-DAB)] bands belonging to ν_s(CN) and δ_s(CH) are not present anymore in the rR spectrum, whereas the metal–metal and metal–ligand stretching as well as the ligand deformation modes below 1000 cm^{-1} are now rather intense [23]. This shows that the SBLCT transition of this complex is again strongly metal–ligand (and possibly also metal–metal) bonding-to-antibonding causing a weakening of the corresponding bonds and a deformation of the Ru–^{i}Pr-DAB metallacycle.

6. Conclusions

The preceding sections gave an overview of the rR spectra of a number of d^6 metal–diimine complexes, with special attention paid to the factors that influence the appearance of these spectra. These factors are: (1) the degree of mixing between the orbitals involved in the electronic transition by dπ–π* and/or σ–π* interaction; and (2) the character of that transition.

Whenever the metal and ligand orbitals strongly mix, either by d$\pi - \pi$* or $\sigma - \pi$* interaction, the symmetric CN stretching vibration is lowered in frequency. If ν_s(CN) is shifted to a frequency lower than ca. 1490 cm^{-1}, a concomitant resonance enhancement of δ_s(CH) (Fig. 4) is observed, as this vibration then obtains some ν_s(CN) character and becomes vibrationally coupled to the electronic transition. As a result of the increase of dπ–π* or σ–π* interaction the electronic transition loses charge transfer character and becomes more metal–ligand bonding-to-antibonding. Stretching vibrations, such as ν_s(CO) and ν_s(CN) become much weaker, and metal–ligand stretching vibrations and deformation modes of the M-DAB metallacycle gain intensity. In extreme cases the ligand stetching modes disappear from the rR spectra and only the low-frequency vibrations give rise to rR effects.

In the case of methyl complexes, an increase of participation of the methyl group in the electronic transition may e.g. occur by a change of character of this transition from MLCT to SBLCT. The symmetric methyl group deformation mode, δ_s(CH$_3$) then becomes strongly enhanced in intensity. Remarkably, the metal–carbon stretching vibration is not resonantly enhanced at all. Hence, the latter vibration is not a good indicator of the character of an electronic transition, in contrast to δ_s(CH$_3$).

A remarkable result of this study is that, while the rR spectra of e.g. [Ru(Cl)(CH$_3$)(CO)$_2$(^{i}Pr-DAB)] and [Ru(SnPh$_3$)$_2$(CO)$_2$(^{i}Pr-DAB)] are very different in appearance, most of these differences can be ascribed to changes in π-interaction between the orbitals involved in the electronic transition rather than attributed to a change in character of this transition. The only indication that a change in character of the electronic transition affects the rR effects of the ^{i}Pr-DAB ligand is

provided by the spectrum of [$W(CO)_4$(^{i}Pr-DAB)] (Fig. 2). This spectrum shows resonance enhancement of Raman intensity for ν(CC)/δ_s(CH) at 1147 cm^{-1}, whereas this band is not observed for any of the other complexes. Apparently, the central CC bond of the ^{i}Pr-DAB ligand is only affected by the electronic transition when it has MLCT character provided the d$\pi-\pi^*$ interaction in the complex is strong.

The DFT calculations were essential for the correct assignment of the resonance enhanced Raman bands. However, it became also clear that if such calculations are performed on structurally simplified model complexes (e.g. replacement of ^{i}Pr-DAB by Me-DAB), this might have a profound influence on the calculated character and frequency of certain vibrations.

Acknowledgements

This work has been undertaken as a part of the European collaborative COST project (D14/0001/99).

References

[1] A.C. Albrecht, J. Chem. Phys. 34 (1961) 1476.
[2] D.L. Rousseau, J.M. Friedman, P.F. Williams, Top. Curr. Phys. 11 (1979) 203.
[3] R.J.H. Clark, B. Stewart, Struct. Bonding 36 (1979) 1.
[4] R.J.H. Clark, T. Dines, Angew. Chem. Int. Ed. Engl. 25 (1986) 131.
[5] A. Myers-Kelley, J. Phys. Chem. A 103 (1999) 6891.
[6] J.I. Zink, K.-S.K. Shin, in: D.H. Volman, G.S. Hammond, D.C. Neckers (Eds.), Molecular Distortions in Excited Electronic States Determined from Electronic and Resonance Raman Spectroscopy. In: Advances in Photochemistry, vol. 9, Wiley, New York, 1991, p. 119.
[7] P. Muraoka, T.W. Bitner, J.I. Zink, Res. Chem. Intermed. 26 (2000) 69.
[8] S.Y. Lee, E.J. Heller, J. Chem. Phys. 71 (1979) 4777.
[9] E.J. Heller, R.L. Sundberg, D. Tannor, J. Phys. Chem. 86 (1982) 1822.
[10] S.O. Williams, D.G. Imre, J. Phys. Chem. 92 (1988) 3363.
[11] D.J. Stufkens, Coord. Chem. Rev. 104 (1990) 39.
[12] B.D. Rossenaar, D.J. Stufkens, A. Vlček Jr., Inorg. Chem. 35 (1996) 2902.
[13] H.A. Nieuwenhuis, D.J. Stufkens, A. Oskam, Inorg. Chem. 33 (1994) 3212.
[14] M.P. Aarnts, D.J. Stufkens, M.P. Wilms, E.J. Baerends, A. Vlček Jr., I.P. Clark, M.W. George, J.J. Turner, Chem. Eur. J. 2 (1996) 1556.
[15] C.J. Kleverlaan, D.J. Stufkens, J. Fraanje, K. Goubitz, Eur. J. Inorg. Chem. (1998) 1243.
[16] C.J. Kleverlaan, D.J. Stufkens, Inorg. Chim. Acta 284 (1999) 61.
[17] J.M. Kliegman, R.K. Barnes, Tetrahedron (1970) 26.
[18] M.J.A. Kraakman, K. Vrieze, H. Kooijman, A.L. Spek, Organometallics 11 (1992) 3760.
[19] M.P. Aarnts, D.J. Stufkens, A. Oskam, J. Fraanje, K. Goubitz, Inorg. Chim. Acta 256 (1997) 93.
[20] S. Hasenzahl, H.-D. Hausen, W. Kaim, Chem. Eur. J. 1 (1995) 95.
[21] J. van Slageren, S. Záliš, A. Klein, D.J. Stufkens, submitted for publication.
[22] J. van Slageren, D.J. Stufkens, Inorg. Chem. 40 (2001) 277.
[23] J. van Slageren, F. Hartl, D.J. Stufkens, Eur. J. Inorg. Chem. (2000) 847.
[24] R. Frech, J.P. Devlin, Chem. Phys. Lett. 38 (1976) 79.

[25] E.J. Baerends, A. Bérces, C. Bo, P.M. Boerrigter, L. Cavallo, L. Deng, R.M. Dickson, D.E. Ellis, L. Fan, T.H. Fischer, C. Fonseca Guerra, S.J.A. van Gisbergen, J.A. Groeneveld, O.V. Gritsenko, F.E. Harris, P. van den Hoek, H. Jacobsen, G. van Kessel, F. Kootstra, E. van Lenthe, V.P. Osinga, P.H.T. Philipsen, D. Post, C.C. Pye, W. Ravenek, P. Ros, P.R.T. Schipper, G. Schreckenbach, J.G. Snijders, M. Sola, D. Swerhone, G. te Velde, P. Vernooijs, L. Versluis, O. Visser, E. van Wezenbeek, G. Wiesenekker, S.K. Wolff, T.K. Woo, T. Ziegler, ADF 1999.01: Amsterdam, 1999.
[26] C. Fonseca Guerra, J.G. Snijders, G. te Velde, E.J. Baerends, Theor. Chem. Acc. 99 (1998) 391.
[27] M.J. Frisch, G.W. Trucks, H.B. Schlegel, G.E. Scuseria, M.A. Robb, J.R. Cheeseman, V.G. Zakrzewski, J.J.A. Montgomery, R.E. Stratmann, J.C. Burant, S. Dapprich, J.M. Millam, A.D. Daniels, K.N. Kudin, M.C. Strain, O. Farkas, J. Tomasi, V. Barone, M. Cossi, R. Cammi, B. Mennucci, C. Pomelli, C. Adamo, S. Clifford, J. Ochterski, G.A. Petersson, P.Y. Ayala, Q. Cui, K. Morokuma, D.K. Malick, A.D. Rabuck, K. Raghavachari, J.B. Foresman, J. Cioslowski, J.V. Ortiz, B.B. Stefanov, G. Liu, A. Liashenko, P. Piskorz, I. Komaromi, R. Gomperts, R.L. Martin, D.J. Fox, T. Keith, M.A. Al-Laham, C.Y. Peng, A. Nanayakkara, C. Gonzalez, M. Challacombe, P.M.W. Gill, B. Johnson, W. Chen, M.W. Wong, J.L. Andres, C. Gonzalez, M. Head-Gordon, E.S. Replogle, J.A. Pople, GAUSSIAN 98, Revision A.6, Gaussian Inc., Pittsburgh, PA, 1998.
[28] D.E. Woon, T.H. Dunning, J. Chem. Phys. 98 (1993) 1358.
[29] D. Andrae, U. Häussermann, M. Dolg, H. Stoll, H. Preuss, Theor. Chim. Acta 77 (1990) 123.
[30] P.J. Stephens, F.J. Devlin, C.F. Cabalowski, M.J. Frisch, J. Phys. Chem. 98 (1994) 11623.
[31] A.D. Becke, Phys. Rev. A 38 (1988) 3098.
[32] J.P. Perdew, Phys. Rev. A 33 (1986) 8822.
[33] M.W. Wong, Chem. Phys. Lett. 256 (1996) 391.
[34] R.W. Balk, D.J. Stufkens, A. Oskam, J. Chem. Soc. Dalton Trans. (1981) 1124.
[35] D.R. Gamelin, M.W. George, P. Glyn, F.-W. Grevels, F.P.A. Johnson, W. Klotzbücher, S.L. Morrison, G. Russell, K. Schaffner, J.J. Turner, Inorg. Chem. 33 (1994) 3246.
[36] A. Vlček Jr., F.-W. Grevels, T.L. Snoeck, D.J. Stufkens, Inorg. Chim. Acta 278 (1998) 83.
[37] R.W. Balk, D.J. Stufkens, A. Oskam, J. Chem. Soc. Dalton Trans. (1982) 275.
[38] L.H. Staal, D.J. Stufkens, A. Oskam, Inorg. Chim. Acta 26 (1978) 255.
[39] P.C. Servaas, H.K. van Dijk, T.L. Snoeck, D.J. Stufkens, A. Oskam, Inorg. Chem. 24 (1985) 4494.
[40] P.C. Servaas, D.J. Stufkens, A. Oskam, Inorg. Chem. 28 (1989) 1774.
[41] B.D. Rossenaar, C.J. Kleverlaan, M.C.E. van de Ven, D.J. Stufkens, A. Oskam, J. Fraanje, K. Goubitz, J. Organomet. Chem. 493 (1995) 153.
[42] G.P. McQuillan, D.C. McKean, C. Long, A.R. Morrison, I. Torto, J. Am. Chem. Soc. 108 (1986) 863.
[43] G.J. Stor, D.J. Stufkens, P. Vernooijs, E.J. Baerends, J. Fraanje, K. Goubitz, Inorg. Chem. 34 (1995) 1588.
[44] M. Turki, C. Daniel, S. Záliš, A. Vlček, Jr., J. van Slageren, D.J. Stufkens, submitted for publication.
[45] W. Kaim, A. Klein, S. Hasenzahl, H. Stoll, S. Záliš, J. Fiedler, Organometallics 17 (1998) 237.
[46] M.W. Kokkes, T.L. Snoeck, D.J. Stufkens, A. Oskam, M. Christophersen, C.H. Stam, J. Mol. Struct. 131 (1985) 11.
[47] M.P. Aarnts, M.P. Wilms, K. Peelen, J. Fraanje, K. Goubitz, F. Hartl, D.J. Stufkens, E.J. Baerends, A. Vlček Jr., Inorg. Chem. 35 (1996) 5468.
[48] J.I. Zink, L. Tutt, Y.Y. Yang, Excited state distortions determined by electronic and Raman spectroscopy, in: A.B.P. Lever (Ed.), Excited States and Reactive Intermediates. In: ACS Symposium Series 307, vol. 38, American Chemical Society, Washington, DC, 1986.